Tribology International 148 (2020) 106322

Contents lists available at ScienceDirect

Tribology International

journal homepage: http://www.elsevier.com/locate/triboint

Measurement of roller load, load variation, and lubrication in a wind turbine gearbox high speed shaft bearing in the field

G. Nicholas [a,*], T. Howard [a], H. Long [a], J. Wheals [b], R.S. Dwyer-Joyce [a]

[a] The Leonardo Centre for Tribology, The University of Sheffield, Sheffield, South Yorkshire, S1 3JD, United Kingdom
[b] Ricardo Innovations Ltd, Midlands Technical Centre, Royal Leamington Spa, Leamington Spa, CV31 1FQ, United Kingdom

ARTICLE INFO

Keywords:
Bearing load and lubrication monitoring
In-situ measurement
Rolling element bearings
Ultrasound

ABSTRACT

The variability of applied load and the integrity of lubrication are crucial factors dictating the durability of wind turbine gearbox bearings. In this work, new ultrasonic reflectometry techniques have been implemented to measure both load and lubrication in the high-speed shaft bearing of a field operational Vestas V42 wind turbine gearbox.

Miniature piezoelectric transducers were bonded onto the bearing outer raceway. The reflected pulses were used to infer bearing load and lubrication. Roller load measurements were seen to vary by 33% across the roller complement, with similar trend observed for reflection coefficient. Inspection of the reflection coefficient patterns were able to show whether the roller inlet region was fully flooded or partially starved, capturing the stochastic behaviour of bearing lubrication.

1. Introduction

For the past decade there has been considerable growth in wind energy for power generation worldwide. This trend is expected to persist as global energy consumption increases [1]. To keep the cost of generation down, wind turbines require good reliability and low cost maintenance. Although electrical components are more prone to failure [2], it is the tribological components such as blade pitch, nacelle yaw systems and gearbox bearings that have a higher repair or replacement cost [3]. Despite a moderate propensity of failure, the wind turbine gearbox accounts for the longest downtime and most costly repairs [4,5]. Most of these failures are a result of degradation of bearing [6]. Improved measurement and understanding of bearing lubrication and loading could help in predicting modes of failures and indications of bearing health that can then be used to organise effective maintenance and minimise unplanned downtime.

Typically, Supervisory Control & Data Acquisition (SCADA) measurements were collected routinely to provide information on the maintenance condition and operational performance of the wind turbine. The data collated are also used in failure prognostics and diagnostics [5]. More cutting-edge condition monitoring systems use vibration and acoustic emissions and oil monitoring techniques alongside SCADA. However, temperature measurements are most commonly used to predict and diagnose failure of wind turbine components [5]. Advanced condition monitoring sensors are not without drawbacks. Acoustic emission sensors are costly and due to their high sensitivity, are susceptible to noise which results in the requirement for extensive signal processing to yield meaningful data. Accelerometers are cheaper but suffer from the same noise problem, which is more profound at low frequencies [7]. Contrarily, on-line oil sensors are expensive and as a result normally periodic manual oil sample measurements are used [7].

Active (i.e. sound generation and receiving, rather than just passive listening) ultrasonic testing methods are utilized in the structural analysis of wind turbine tower and blades but as yet not in the gearbox [8,9]. Sound wave pulses are transmitted into the composite components and the echoes or reflections received can be analysed to deduce the thickness of different layers of, for example, composite laminate and thus the potential to detect delamination [10].

Previously, ultrasonic measurements have been successfully trialled and implemented, within the laboratory environment, on rolling element bearings for both lubricant film thickness [11,12] and contact load measurement [13] with good accuracy. However, these approaches are yet to be used in a field environment to explore both durability and how real wind dominated operation affects signals and bearing performance.

In the current study, ultrasonic measurements of a high-speed shaft

* Corresponding author.
E-mail address: gnicholas1@sheffield.ac.uk (G. Nicholas).

https://doi.org/10.1016/j.triboint.2020.106322
Received 25 October 2019; Received in revised form 17 March 2020; Accepted 19 March 2020
Available online 24 March 2020

bearing obtained from a gearbox within an operational wind turbine are presented. The current research aims to show the capabilities of ultrasound to provide better comprehension of bearing roller load and lubrication under actual turbine operational conditions.

2. Ultrasonic measurement principles

2.1. Ultrasonic reflection at a lubricated interface

When an ultrasonic pulse strikes an interface between two dissimilar materials, a portion of its energy is transmitted through whilst the remaining is reflected back. The proportion of the wave amplitude reflected, known as the reflection coefficient, *R*, depends on the acoustic mismatch of two materials and is given by:

$$R = \frac{z_2 - z_1}{z_2 + z_1}, \quad z = \rho c \tag{1}$$

where ρ and c are density and speed of sound within media 1 and 2 either side of the interface.

Fig. 1 shows examples of various interfaces that ultrasonic waves strike, with an illustration of their respective reflection coefficient values. If the two bodies are of perfectly bonded very similar materials, such as different grades of steel (Fig. 1a) then most of the pulse will be transmitted through and the reflection coefficient would be close to zero. Conversely, if the two bodies are acoustically dissimilar, such as steel and air (Fig. 1b), almost all of the pulse will be reflected back and *R* will be unity. For a steel and free surface lubricant interface shown in Fig. 1c, around 95% ($R = 0.95$) of the energy will be reflected back and the remaining portion transmitted through the oil film.

Fig. 1d shows a thin oil film between two bodies. In this case reflections occur at both interfaces, but in practice the oil film is so thin that these reflections superimpose. Various methods exist for ultrasonic measurement of the lubricant film thickness [11,14–17]. For lubricant films thicker than around 40 μm, the reflected pulses from the two sides of the oil interface can still be distinguished and thus time-of-flight (ToF) and resonance methods [18] can be applied.

For thin lubricant films of less around 20 μm, the film can be treated as a distributed spring with stiffness, *K* which the reflection coefficient, *R* will be dependent upon according to the relationship:

$$R = \frac{z_1 - z_2 + i\omega\left(z_1 z_2 / K\right)}{z_1 + z_2 + i\omega\left(z_1 z_2 / K\right)}, \quad K = \frac{B}{h} \tag{2}$$

where ω is the angular frequency of the ultrasonic sensor, *B* is the bulk modulus of the lubricant film and *h* is the lubricant film thickness [11]. Substituting *K* into *R* and rearranging for lubricant film thickness, *h* gives:

$$h = \frac{\rho c^2}{\omega z_1 z_2}\sqrt{\frac{|R|^2(z_1 + z_2)^2 - (z_1 - z_2)^2}{1 - |R|^2}} \tag{3}$$

Ultrasonic measurements of lubricant film thickness have been conducted in rolling element bearings within the elastohydrodynamic regime [15,17,19,20]. Due to the small contact dimensions between the rolling element and raceway, the ultrasonic waves are required to be focused to ensure that the ultrasonic beam falls within the contact patch. This requires modifications to the bearing raceway to accommodate a concave lens and water bath and this is not currently practical in a field application. Further, in the relatively slow moving bearings in a wind turbine, it is likely that much of the operation is in the mixed lubrication regime. The presence of steel-oil and steel-steel asperity contact regions within the interface complicates oil film measurement [21].

As a consequence, conversion of reflection coefficient into lubricant film thickness was not conducted in this study and reflection coefficient was used instead only as an empirical indicator of lubricant presence.

2.2. Inferring raceway deflection from the reflected time of flight measurements

Fig. 2 schematically shows ultrasonic pulses propagating through an outer raceway. When a roller is not directly present under the sensor (Fig. 2a) all the ultrasonic pulses are reflected back from a nominally unstressed, un-deformed region of the raceway. Conversely, when a roller travels past the sensing location (Fig. 2b), it reduces the ultrasound transmission path and contributes to a ToF change. Variation in ToF can then be used to infer raceway deflection and hence load. A brief summary of the method is outlined below; full details can be found in Ref. [13].

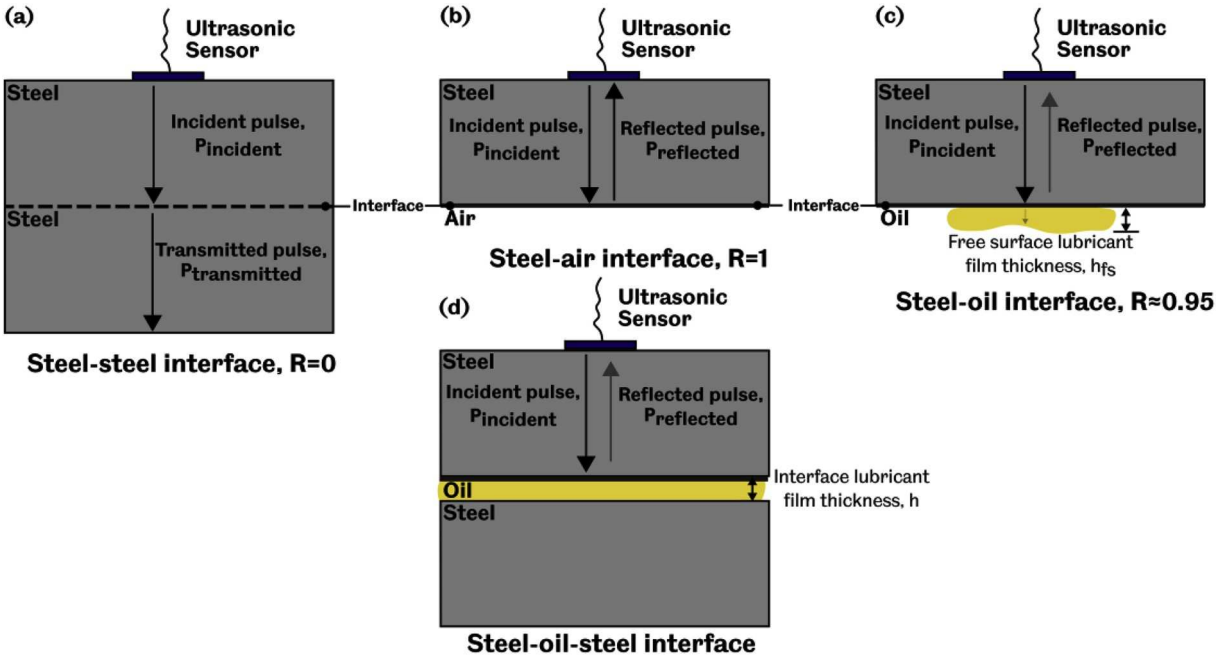

Fig. 1. Ultrasonic reflections from various interfaces: a) fully bonded steel-steel interface b) steel-air interface c) steel-oil interface d) steel-oil-steel interface.

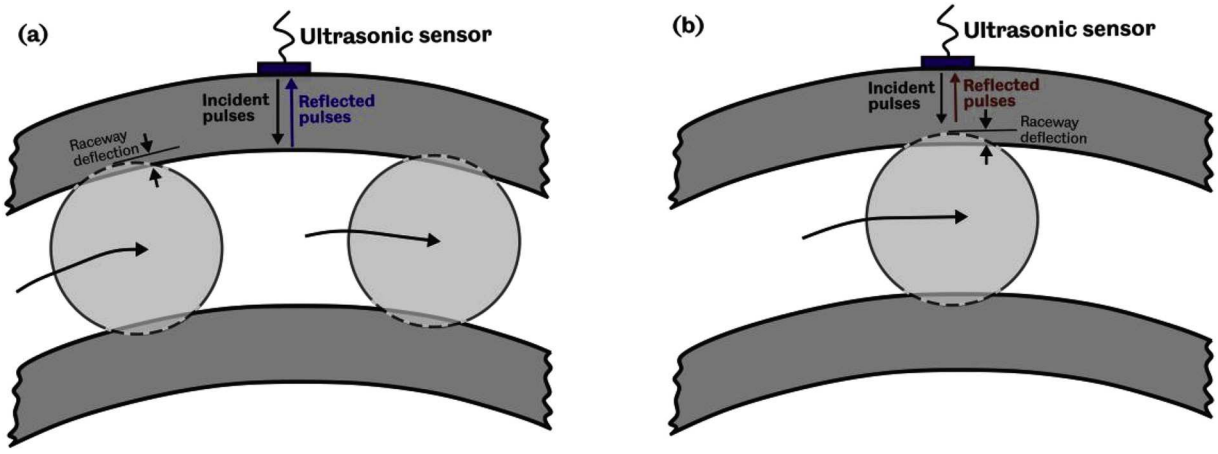

Fig. 2. Ultrasonic transmission through an outer raceway for a) when roller is remote from the sensor (raceway portion unloaded) and b) when roller is directly beneath sensor (raceway portion loaded).

The total ToF change, Δt for a rolling bearing contact under load arises from three sources: surface deflection, variation in sound speed with stress (the acoustoelastic effect), and an apparent change in ToF due to a phase change at the interface [13]. Mathematically this is given by Ref. [13]:

$$\Delta t = \frac{2(1 - L_{zz})\delta}{(c_{zz})_0} + \frac{\varnothing_R}{2\pi f} \tag{4}$$

where $(c_{zz})_0$ is the speed of sound in the unloaded raceway, δ is the raceway deflection, $\varnothing_R$ is the phase change between the loaded and unloaded signal, and f is the centre frequency of the ultrasonic wave. L_{zz} is the acoustoelastic constant which defines the change in speed of sound with stress in the material. It is usually determined through experiment, for bearing steel found to be around −2.24 [13],

The first term includes the two contributions from the raceway deflection and the speed of sound change. The second term describes the apparent ToF change caused by a phase change. By taking the Hilbert Transform of the pulse and obtaining its energy profile, the second term of (4) can be negated, leaving only the first term [13].

After inferring the raceway deflection from Δt measurements using equation (4), appropriate contact models can be applied to convert deflection measurements to contact load.

2.3. Deducing roller load from raceway deflection

Using an appropriate elastic contact model based on the materials and geometries of the raceway and rolling element, the roller contact load can be obtained from raceway deflection. As rollers are typically crowned or have a certain transverse profile, line contact does not exist across the full load spectrum. The contact typically is point or elliptical at low loads and gradually transitions into a line as the bearing load increases [22].

Houpert's relationship [22] considered this transition and defined a deflection, δ_{trans} where the contact shifts from elliptical to line which can be evaluated using the following relationships:

$$\boldsymbol{\delta_{trans}} = \left(\frac{1.078}{1.5}\cdot\frac{\boldsymbol{K_{LC}}}{\boldsymbol{K_{PC}}}\right)^{1/0.422} \tag{5}$$

$$\boldsymbol{K_{PC}} = \frac{\boldsymbol{E'}\sqrt{\boldsymbol{R_x}}}{\boldsymbol{C_1^{1.5}}\cdot\boldsymbol{k}^{\boldsymbol{C_2}\cdot 1.5}}, \quad \boldsymbol{K_{LC}} = 0.2785\cdot\boldsymbol{E'}\cdot\boldsymbol{L}\left(\frac{1+\gamma_o}{t}\right)^{0.078} \tag{6}$$

where K_{PC} and K_{LC} are point and line contact constants which are a function of bearing geometry, E' and R_x are the reduced modulus and reduced radius in x-direction respectively, L is the effective roller length, t is the thickness of the outer raceway, C_1 and C_2 are elliptical integral constants (for this study, $C_1 = 1.7138$ and $C_2 = -0.2743$ [22]) which vary with k, the ratio of reduced radius in y-direction to that of the x-direction, and γ_o is the half included centre line angle. C1 and C2 values were obtained through curve-fitting with a difference of <1% from numerical values. A more accurate and sophisticated curve-fitting exist [23] with an error of <0.05%. As only <1% error exist for the current constants, this would have minor effect on the load measurements.

If the deflection, δ is less than the transitional deflection, δ_{trans} the contact will remain elliptical and (7) is used to calculate maximum roller load, Q:

$$\boldsymbol{Q} = \boldsymbol{K_{PC}}\cdot(2\boldsymbol{\delta})^{1.5} \tag{7}$$

whereas equation (8) is used for the deflection values that exceed the transitional deflection:

$$\boldsymbol{Q} = \boldsymbol{K_{LC}}\cdot(2\boldsymbol{\delta})^{1.078} - \boldsymbol{dQ} \tag{8}$$

where dQ is defined by:

$$\boldsymbol{dQ} = \left(\frac{1.078}{1.5}\cdot\frac{\boldsymbol{K_{LC}}}{\boldsymbol{K_{PC}}}\right)^{1.1/0.422}\cdot\left(\frac{0.422}{1.5}\cdot\boldsymbol{K_{LC}}\right) \tag{9}$$

In this study, the measured bearing loads were found to be low (less than 10% of the bearing dynamic load rating). Through comparison of the transitional deflection calculated using equation (5) with the ultrasonic deflection measurements, the contact was found to be always elliptical with the constant K_{PC} calculated at 1.796E+11.

The total ToF change, Δt is obtained from ultrasonic measurements; the speed of sound in the raceway, $(c_{zz})_0$ and the acoustoelastic constant, L_{zz} are known. Combining equations (4), (6) and (7) gives the maximum roller load:

$$\boldsymbol{Q} = \boldsymbol{K_{PC}}\left[\frac{\boldsymbol{\Delta t}(\boldsymbol{c_{zz}})_0}{(1-\boldsymbol{L_{zz}})}\right]^{1.5} \tag{10}$$

This maximum roller load can then be determined from recorded reflection measurements for each roller within the bearing complement during bearing rotation.

3. Instrumentation and methodology

3.1. Gearbox bearing selection

In this study, a gearbox bearing from a fully operational 600 kW Vestas V42 wind turbine (WT) was instrumented. The turbine was one of

several in the Barnesmore wind farm located in Donegal, Ireland. Instrumentation was made possible due to scheduled maintenance of the gearbox which necessitates its removal from the nacelle and transportation to an off-site facility, allowing for access to the high-speed shaft tapered roller bearing (TRB).

Key specifications of the WT gearbox and the selected bearing are shown in Table 1. Fig. 3 shows the instrumented high-speed shaft tapered roller bearing (marked as **B**) within the gearbox, selected as it was believed to be the higher loaded of the two TRBs. The high speed shaft bearing was lubricated with a VG320 gear oil.

3.2. Bearing instrumentation

For ultrasonic pulse generation and receiving, piezo-electric elements were bonded onto the bearing outer race. Fig. 4 shows the positions of the two ultrasonic sensors and a schematic of the ultrasonic data acquisition hardware. One sensor (CH1) was positioned at the edge of the maximum loaded region whilst the other (CH2) directly within the maximum loaded region. The sensors operated in pulse-echo mode and an ultrasonic pulse receiver was used to excite the piezoelectric elements. The reflected signals were captured, digitized by the data acquisition system at 100 MHz and streamed to the computer for storage. Within the capture window, 1 s of ultrasonic pulses were captured every 20 min, at a pulse repetition rate (PRR) of 80 kHz. The high PRR was necessary due to the high rotational speed of the bearing (1500 rpm) and subsequently the speed at which each roller would pass across the ultrasonic elements. The 20 min delay was implemented between capture instances to avoid occupying too much storage space, as one of the datasets occupied 50 MB of disk space. In this way, for each sensor, 8×10^6 data-points were recorded at 0.01 μs intervals for 1 s every 20 min of turbine operation.

The piezo-ceramic discs used in this study were of 10 MHz central frequency. The procedure for sensor installation onto the outer race is outlined in Fig. 5. The discs had a diameter of 7.1 mm and thickness of 0.2 mm. To enhance their spatial resolution (i.e. by reducing their size), they were cut into rectangular strips of 5×1 *mm*. To accommodate the sensors and wiring, a groove parallel to the rolling contact surface was machined. The parallel groove was necessary so that sound waves generated by the sensors would strike the contact surface perpendicularly and thus be reflected straight back as shown in the bottom right sketch in Fig. 5.

Next, the sensors were bonded onto the parallel surface with a high performance strain gauge epoxy. The upper operational limit of the strain gauge epoxy used was 250 $^{\circ}C$ sufficiently above the expected operational temperature of the bearing ($\sim$50 $^{\circ}C$). Thermocouples were installed adjacent to the ultrasonic elements to provide the closest record of the temperatures occurring at the contact under observation by each ultrasonic element. Finally, the piezo-ceramic strips were wired with shielded coaxial cable and covered with a protective layer of high temperature epoxy.

4. Analysis procedure

Fig. 6 schematically shows the various ultrasonic reflections recorded from a sensor (an A-Scan). The blue signal depicts the reflections

Table 1
Key specifications of the WT gearbox & instrumented bearing.

Gearbox Type	Hansen EH55G21S-BN-50 (Planetary)
Gearbox Stages	3
Gearbox Ratio	1:50
Maximum high-speed shaft speed	1500 rpm
High Speed Shaft Bearing Type	32222 Tapered Roller Bearing
No. of Rollers, Z	20
Outer raceway contact angle, ϕ	15.64°

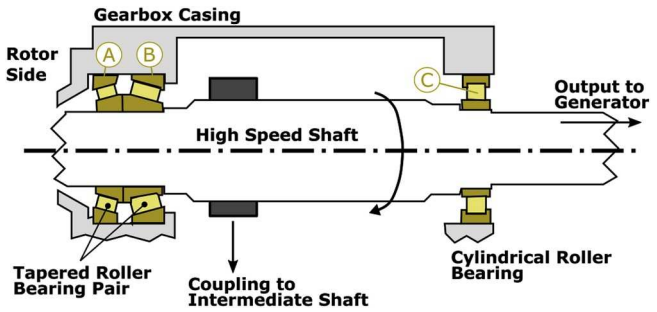

Fig. 3. High speed shaft bearing configuration [24].

obtained when a roller is not directly under the sensor or when the raceway portion is unloaded, whilst the red signal captures reflections when the raceway portion is loaded.

Referring to the waveform in Fig. 6, the first pulse recorded is the initial excitation sent to excite the transducer. The subsequent pulses are the first, second and third reflections from the raceway-roller interface. Although not used in this work, it is interesting to observe the reflection from the opposite roller interface; the pulse has travelled through the outer raceway-roller contact and been reflected from the inner raceway-roller contact.

The first reflection from the raceway interface provides the best signal to noise ratio and was selected for further processing; a window was assigned over it. Fig. 7 shows the raw ultrasonic datastream consisting of an assembly of each first interface reflected pulse obtained from the sensor CH1. The datastream consists of a series of reflected pulses plotted alongside their respective capture time. Due to their rapid capture rate, the datastream forms a dense compact shape with the pulse peak amplitudes determining the bounds. A magnified view of a section of the datastream shows four reflected interface pulses with very similar pulse shape.

In the data stream shown in Fig. 7 two dips in signal amplitude can be observed; these are caused by roller passes. When a roller is directly within the sensor transmission path, a portion of the ultrasonic energy is transmitted through the roller and thus causes a reduction in signal amplitude. In the gap between the roller passes, a subtle reduction in pulse amplitude can also be observed. This is a result of a change in the lubrication condition of the bearing surface and will be discussed further in §4.3.

4.1. Data processing for reflection coefficient and ToF

Fig. 8 shows the data processing scheme applied to the interface reflected pulses to obtain the reflection coefficient and raceway deflection. The reflection coefficient is defined as the reflected wave amplitude divided by the incident wave amplitude. In practice it is easiest to obtain the incident wave amplitude by recording a reflection from a steel-air interface (since in equation (1) $z_2 >> z_1$ and R approaches unity). This is known as the reference pulse. Within the captured data stream, a reference pulse was extracted as the most frequently occurring pulse within the dataset, coinciding with the instances where raceway-air contact exists.

Two routes for data processing were followed: time-of-flight processing was used to extract the sound path length and hence deflection and load, amplitude processing was used to understand the amount of sound transmitted into the rollers and oil to explore lubrication conditions.

For amplitude based processing, a Fast Fourier Transform was performed on the captured pulses. A reflection coefficient spectrum was then obtained by dividing the spectral amplitude of the measurement pulse, A_m with that of the reference A_r.

ToF based processing to obtain the roller contact load has more steps. A Hilbert Transform was initially performed on both the reference and

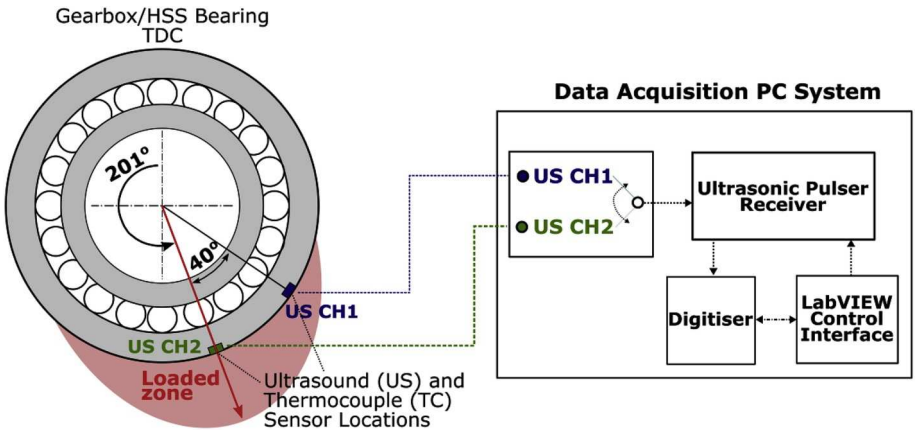

Fig. 4. Schematic of sensor location and data acquisition hardware [24].

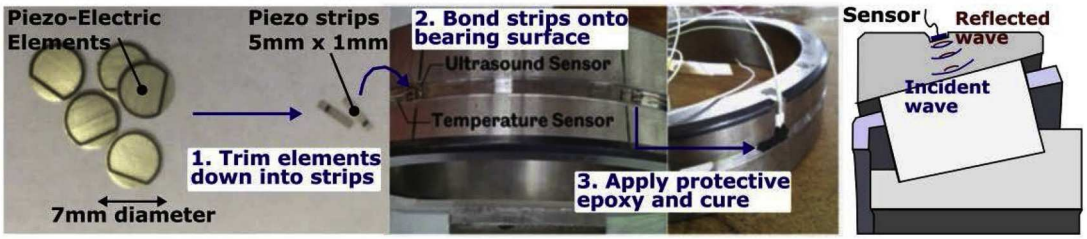

Fig. 5. Ultrasonic sensor instrumentation process.

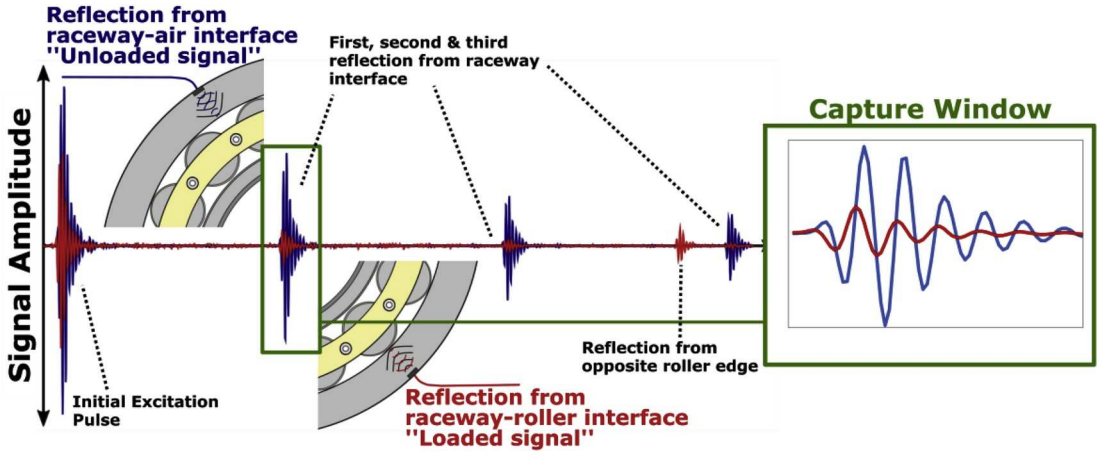

Fig. 6. Raw ultrasonic reflections from various interfaces within the bearing and the extraction of the first raceway/roller interface reflection.

loaded ultrasonic pulses to obtain their envelopes. As the time shift is computed to the closest sampling point, the accuracy of the method is limited to the ultrasonic pulse sampling frequency of 100 MHz. Thus, to improve the accuracy, interpolation was performed on both the reference and loaded envelopes to increase resolution. A sampling frequency of 100 MHz corresponds to digitisation of 10 ns without interpolation or 0.1 ns with a 100 point interpolation. The envelopes were then normalized with their respective maximum amplitudes before performing cross correlation to obtain the time shift. The acoustoelastic correction and the elastic contact equations described in §2.3 were then applied to obtain the load corresponding to the measured time shift.

Fig. 9a and b shows the reflection coefficient and roller load measurements for 3 successive roller passes as recorded by sensor CH1. Dips within the reflection coefficient plot and peaks within the roller load plot correspond to roller passes. The data shows R increasing from 0.95 between roller passes, rising to a maximum at 1.1 or so and then falling to a minimum at 0.7 before rising again. Strictly, R should not rise above 1; these peaks at the contact entry and exit area are caused by interference fringes associated with the finite size of the sensor with respect to the contact region. In this work, due to the low loading on the bearing, the contact patch was smaller than the transducer measurement region (this phenomenon is discussed further in Ref. [15]). This is also the reason for the M-shaped roller load plot shown in Fig. 9b. The method is thus best applied onto large bearings with bigger contact patches. Despite such issues, as shown from the results obtained, meaningful measurements can still be obtained.

From the measurement region which corresponds to the roller passes, the minimum reflection coefficient, R_{min} and the peak roller load, Q_{max} are extracted for each roller pass to be used for further analysis.

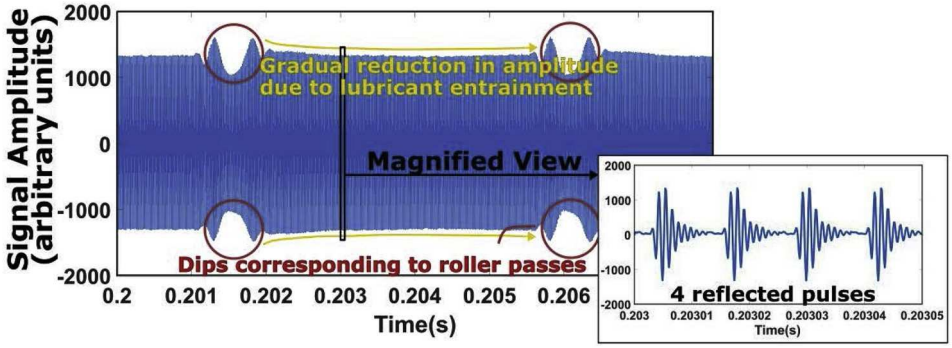

Fig. 7. Datastream consisting of a series of first interface reflected pulses recorded by sensor CH1. The insert shows a magnified section showing four such pulses. As a roller passes over CH1 the reflected pulse is reduced in magnitude. Two such roller passes can be seen in this stream of data.

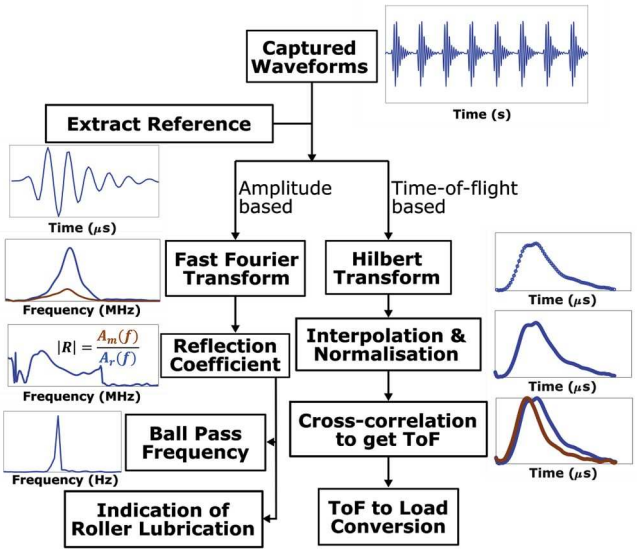

Fig. 8. Schematic diagram showing the processing of captured reflection data using either time-of-flight or amplitude based methods.

4.2. Inferring bearing rotational speed

As roller passes manifest as dips in reflection coefficient, this can be exploited to measure ball pass frequency, which in turn can be used to infer the bearing rotational speed, ω_{brg} given by:

$$\omega_{brg} = \frac{120 \cdot f_o}{Z\left(1 - \frac{d}{D}cos\phi\right)} \tag{11}$$

where f_o is the outer race ball pass frequency, Z is the number of rollers, d and D are the mean roller and pitch diameter respectively and ϕ is the cup angle. By computing the power spectral density for the reflection coefficient (Fig. 9c), the ball pass frequency was found. The power spectral densities for both channels CH1 and CH2, show peaks close to 220 Hz, corresponding to the expected maximum bearing rotational speed of 1500 *RPM*.

4.3. Indication of roller lubrication

As mentioned in §2.1, and shown schematically in Fig. 1c, reduction in the reflected signal amplitude is caused by the presence of lubricant on the bearing contact surface. This effect can be clearly seen in the reflection coefficient data recorded in the gap between rollers. A starved

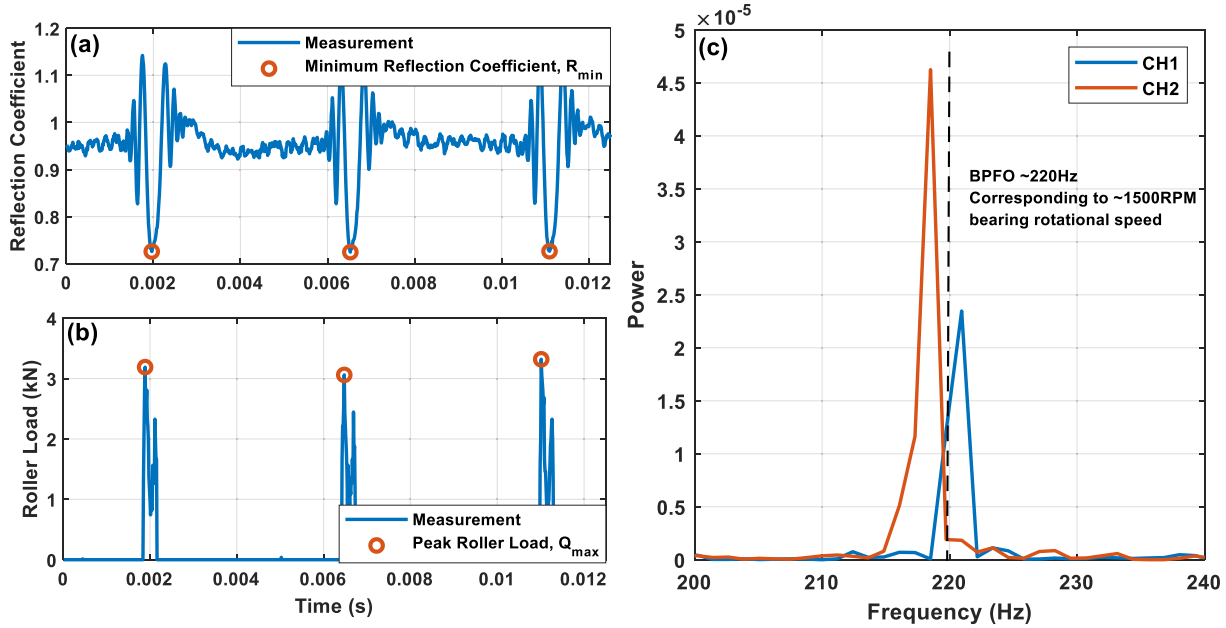

Fig. 9. a) Reflection coefficient and b) roller load measurements for 3 roller passes from CH1 and c) power spectral density of reflection coefficient.

bearing surface (steel-air interface), according to equation (1), will have a reflection coefficient of unity, whilst for a well lubricated surface (steel-oil) we expect a reflection coefficient of 0.95. Figs. 10 and 11 show these features for low and high bearing rotational speeds respectively.

In Fig. 10, for low rotational speeds after a roller pass, the raceway is swept clean of lubricant. This results in a steel-air interface and subsequently a reflection coefficient of unity. For a period of time, the raceway surface remains clean of lubricant. The reflection coefficient then reduces from 1 to around 0.95 as lubricant flows back into the region at a steel-oil interface.

Fig. 11 shows the lubrication behaviour at high bearing rotational speed. The region where $R = 1$ is significantly shorter than that from a slow bearing rotation shown in Fig. 10. After a roller pass, the reflection coefficient immediately begins to drop to 0.95 as the lubricant ahead of the incoming roller is pushed ahead into the region previously swept clean by the prior outgoing roller. The sensitivity of the measurement is theorised to be frequency dependant and also dependant on the thickness of the free surface lubricant film. This was based off equation (12), where h is the free surface lubricant film, c is the speed of sound in the lubricant, and f_m is the resonant frequency of the m-th mode [18].

$$h = \frac{cm}{2f_m} \tag{12}$$

As the sensor's central frequency increases, the free surface lubricant film thickness would decrease. It would also be sensible to assume that the film thickness required to register a reflection coefficient of 0.95 would also reduce. As such, sensor frequency dictates the minimum detectable amount of lubricant, too thin of a lubricant would register a reflection coefficient >0.95. For typical gearbox lubricant (VG320), longitudinal sensors of 10 MHz work particularly well in characterising lubricated and unlubricated instances. The limitation in this instance would be its sensitivity range of 0.95–1.00.

5. Results and analysis

The following sections present ultrasonic measurements obtained from the high-speed shaft bearing. Measurements shown were from a single dataset randomly selected from the constant speed region when the turbine is rotating at its rated speed of 1500 *RPM*, with a generator power and torque of 356 kW and 2200 Nm respectively.

5.1. Reflection coefficient & roller load measurements

Fig. 12 shows the average minimum reflection coefficient values for each of the 20 rollers obtained from CH1 and 2 respectively. The error bars shown represent the range (i.e. the maximum and minimum values recorded for each roller), with each roller having 5 measurements as the bearing completes 5 consecutive revolutions within the 1 s acquisition time. The range measurement is discussed further in §5.3. As expected, measurements from CH1 are higher, with an average of 0.767 compared to 0.733 of CH2 as it experiences lower loading and thus is expected to have a thicker lubricant film and less contact.

The raw measurements were taken without any information about the angular position of the bearing – so it was not possible to identify which roller in the compliment corresponds to which reflection measurement. However, clear recurring patterns within the plots can also be observed, i.e. increasing and decreasing trends of individual roller measurements across the two sensor channels, particularly Roller 18 ($i = 18$) which showed the highest R_{min} values for both channels. These patterns were used to align measurements between the two channels.

Fig. 13 shows the average peak roller load, Q_{max} measurements for the full bearing complement calculated using equation (10) and its range for both channels. Again a full bearing complement data is shown in the graph corresponding to 20 rollers occurring over 5 consecutive revolutions.

Measurements from the sensor located directly within the maximum loaded region (CH2) are clearly higher with an average of 4.360 kN across the complement compared to that of 3.350 kN (CH1). Despite having larger range values within the load measurements, recurring patterns similar to that seen within Fig. 12 can still be observed. Expected trends between the R_{min} and Q_{max} measurements for each roller are also noticed. As an example, Roller 18 registered the lowest Q_{max} for both channels and had the highest R_{min} values across the complement. This is as expected, as the roller carrying the lowest load would have the thickest oil film, less or no solid contact, and hence more reflection.

5.2. Circumferential distribution of roller load

As there are two ultrasonic sensors positioned around the bearing circumference, partial information on the circumferential load distribution can be inferred. The angular variation of the load on a roller can

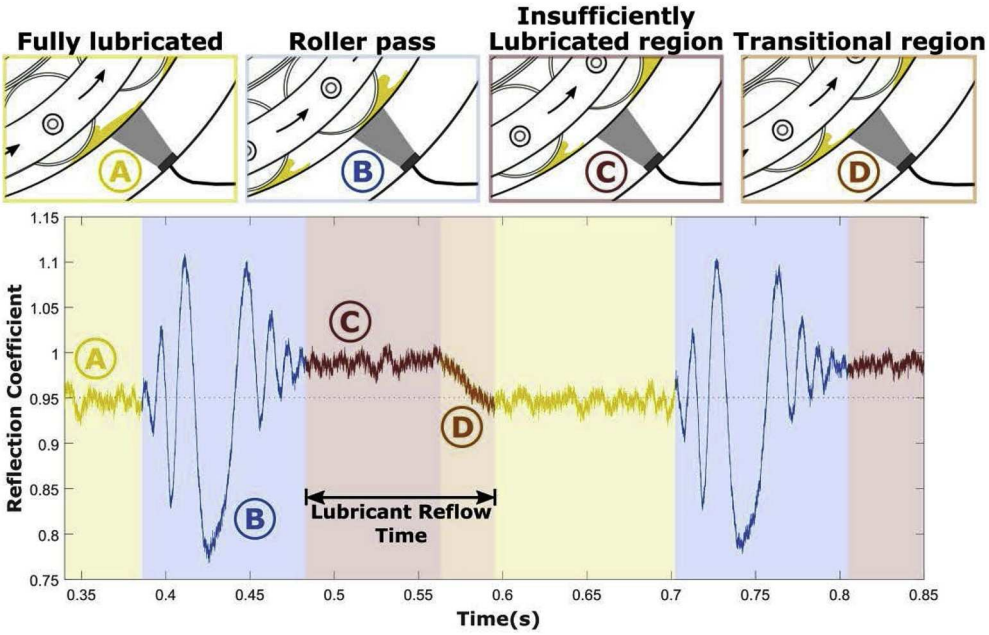

Fig. 10. Lubricant behaviour between roller passes under low rotational speed.

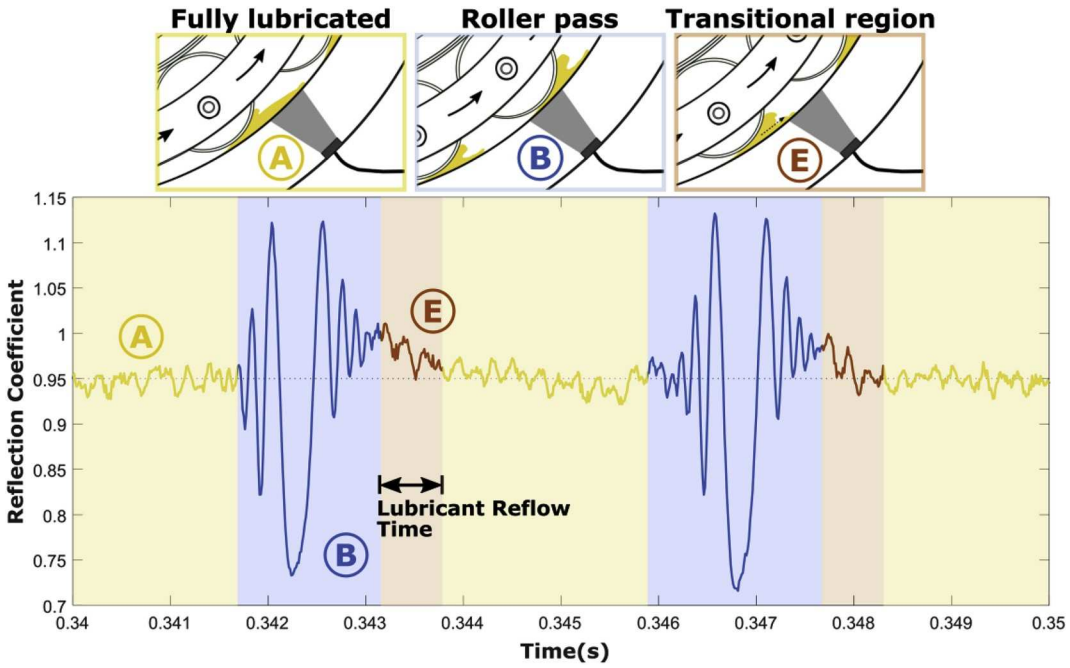

Fig. 11. Lubricant behaviour between roller passes under high rotational speed.

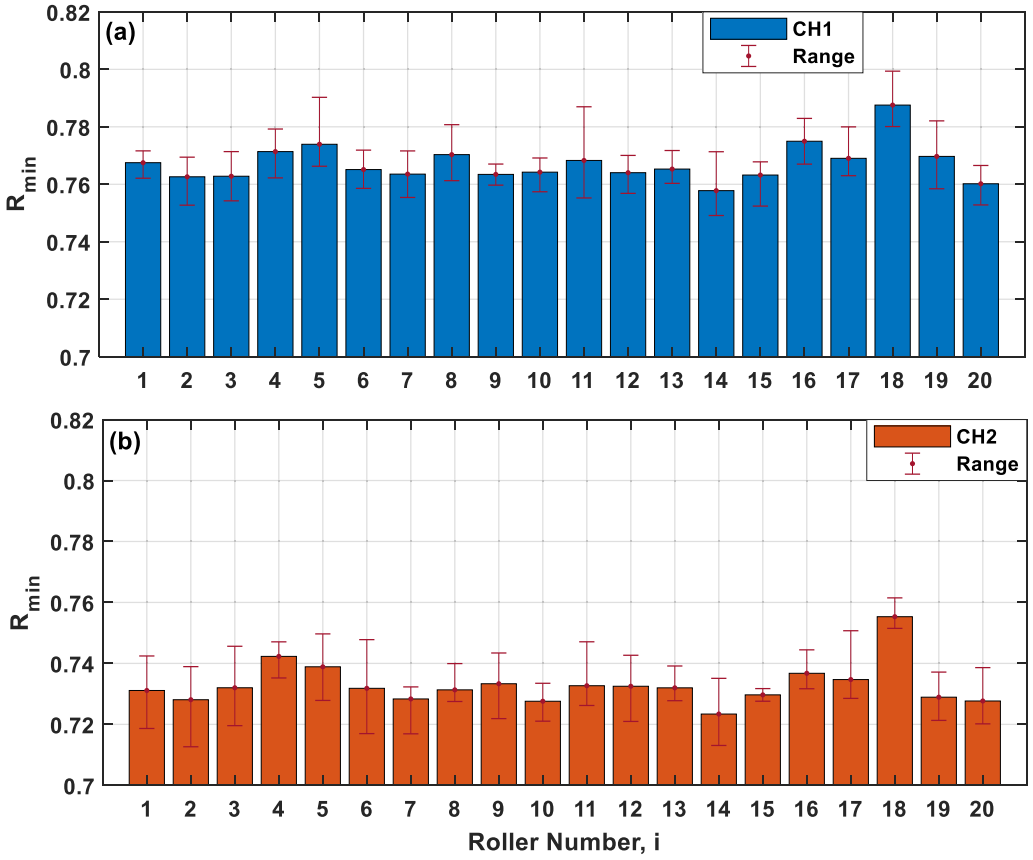

Fig. 12. Average minimum reflection coefficient over 5 consecutive bearing revolutions for each roller for the sensor located at (a) the edge (CH1) and (b) the centre (CH2) of the maximum loaded zone.

be obtained from Ref. [25]:

$$\frac{Q_\phi}{Q_{max}} = \left[1 - \frac{1}{2\varepsilon}(1 - \cos\phi)\right]^{1.5} \tag{13}$$

Q_ϕ and Q_{max} are the roller load at angle ϕ, and the maximum roller load respectively, ϕ is the angle measured from the maximum loaded roller, and ε is related to the radial and axial ring shift of the bearing which was assumed to be 0.5.

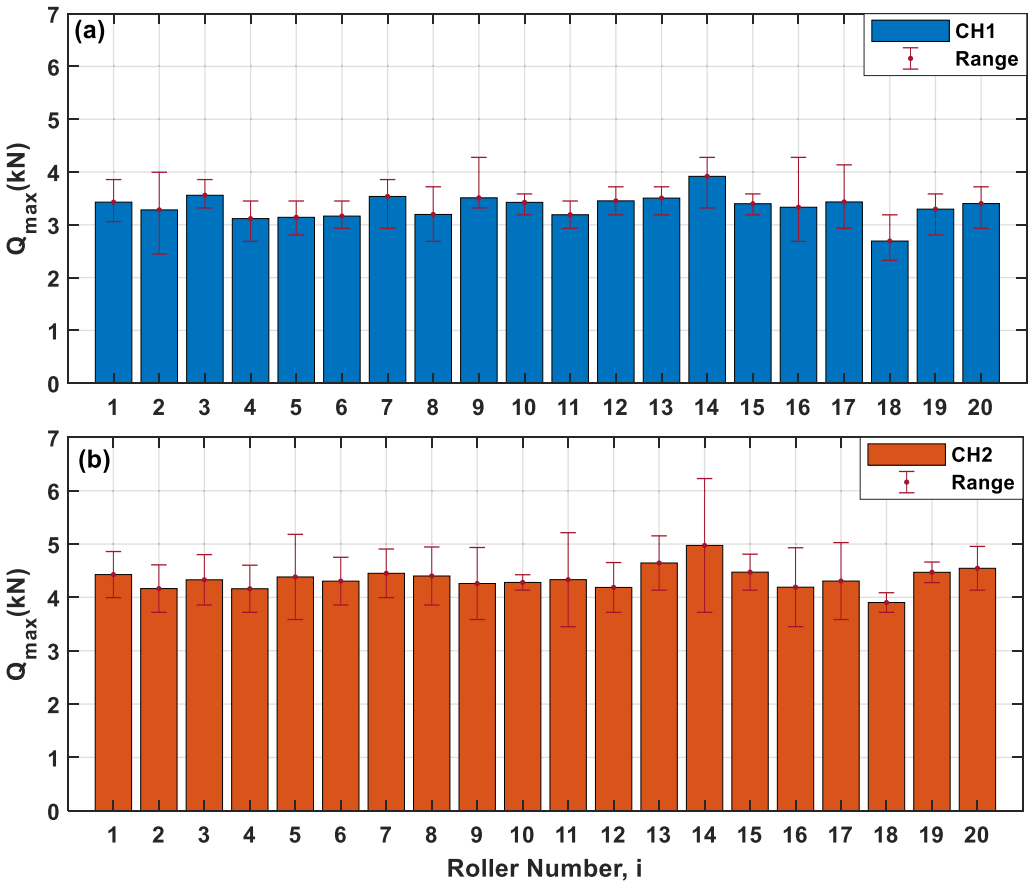

Fig. 13. Average maximum roller load measurements over 5 consecutive bearing revolutions for each roller for the sensor located at (a) the edge (CH1) and (b) the centre (CH2) of the maximum loaded zone.

For the conditions in this bearing and the sensor location, the theoretical ratio was found to be 0.67. This is plotted on Fig. 14c. The average measured ratio was 0.77, both having a difference of around 15%. A reasonable correlation is observed.

5.3. Variation of roller ultrasonic reflection and load

Fig. 14 shows the range measurements of R_{min} and Q_{max} that have been collated and converted into boxplots. For each channel, two range data were compared, the range for a single roller, *i* and the range for all the rollers (cycle), *n*. The range for a single roller, *i* consists of 20 range values for rollers 1 to 20. The range for the cycle, *n* consists of 5 range values for full bearing revolutions 1 to 5.

The reflection coefficient measurements for a single individual roller across 5 cycles ($n = 1$ to 5), e.g. the measurement of roller 18 ($i = 18$) for rotational data, $n = 1$ to 5, is very consistent with an average range of

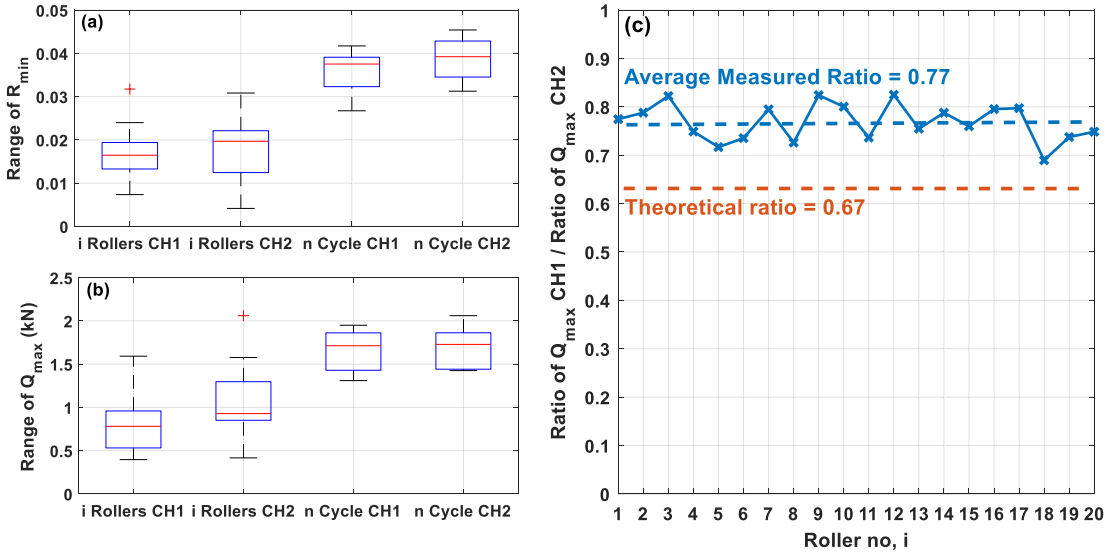

Fig. 14. Variation of a) minimum reflection coefficient and b) peak roller load and c) the ratio of peak roller load of CH1 against CH2.

recorded values (max-min values) of around 0.018 for both channels.

Measurements across a full rotation, i.e. $n = 1$ comparing the measurement of the rollers from $i = 1$ to 20, show a higher range value of 0.036 (CH1) and 0.039 (CH2). These measurements suggest that there seems to be little variation in measurements for the same roller within a compliment but higher variability in measurements obtained from each roller across a cycle within a compliment.

The average range of load measured for the individual rollers ($i = 1$ to 20) was found to be 0.81 kN (CH1) and 1.05 kN (CH2) whilst the average range of load measured across cycles ($n = 1$ to 5) was at 1.65 kN (CH1) and 1.71 kN (CH2). The result suggests again that there is less variation in load carried by the same roller between cycles compared to measurements from each roller within the bearing complement.

It is difficult to say with certainty what causes the variation in load supported by each roller. However the following evidence from this data strongly suggests that it is caused by geometrical differences between the rollers:

(i) The variation in measured load and reflection is significantly less between rollers than it is between cycles.
(ii) Load and reflection measured for each roller correspond; i.e. a high load on a roller is commensurate with a low reflection caused by a thinner oil film and more metal to metal contact.
(iii) The pattern of variation of both load and reflection across the complement ($i = 1$ to 20 for a single cycle $n = 1, 2, 3...$) matches up for both sensors CH1 and CH2. This indicates that a roller passing over CH1 resulting in a peak load is also registering a peak as it passes over CH2. The fact that each sensor (CH1 & CH2) shows the same sequence of load variation, strongly suggests that the load variation is caused by geometrical differences between the rollers.

These geometrical differences between the rollers maybe variation in roller diameter, concentricity between the rotating parts, or differences in roller profiles. Since it has not been possible to extract the actual roller bearing from the turbine, the above is speculation at this stage.

To further investigate the effects of a profile variation on roller load, a simple theoretical study was conducted. An increase or decrease in roller profile height, z will affect the reduced radius in the transverse direction, R_y and subsequently the equivalent radius ratio, k and constant K_{pc}. In the calculation, a roller profile height of 15 μm was assumed to be the design height with a tolerance of ±10 μm. Table 2 shows the predicted variation in roller load, determined using the elastic contact analysis of section 2.3, for several different profile heights. An increase in roller profile height from its design height will result in a decrease in roller load for a fixed amount of deflection. However, a decrease in roller profile height will increase the roller load with a greater rate.

Clearly, an increase in roller load will be detrimental to the bearing. The L_{10} life rating, is a function of the roller load to the power of 10/3 for typical roller bearings [26]. Taking the worst case scenario considered here of −10 μm off design profile height, this will give nearly 1.6 times increase in roller load and subsequently at least 4.5 times decrease in basic bearing L_{10} life rating.

Table 2
Variation of roller load with roller profile height.

Roller profile height, z (μm)	Reduced radius in lateral direction, R_y	Equivalent radius ratio, k	Constant, K_{pc}	Ratio of roller load for various profile height against roller load at design profile, Q/Q_{design}
5	29.86	2279.43	2.83E+11	1.57
10	14.93	1139.72	2.13E+11	1.18
15	9.95	759.81	1.80E+11	1.00
20	7.46	569.88	1.60E+11	0.88
25	5.97	455.89	1.46E+11	0.81

5.4. Variation of reflection coefficient and roller load with rotational speed

Fig. 15 shows the variation of minimum reflection coefficient and maximum roller load with the bearing rotational speed for both CH1 & CH2. Measurements over 1900 datasets of rotational speeds between 0 and 1550 RPM were collated to provide an overview of the trends of minimum reflection coefficient and maximum roller load across varying rotational speeds.

Generally, as the bearing speed increases (and the load remains unchanged) one would expect the reflection coefficient to increase as a thicker oil film forms. This can broadly be seen in Fig. 15a. However, in normal operation the bearing load does not remain constant as the turbine speed increases. Two regimes of turbine operation can be observed:

(i) Transitional (0–1499 *RPM)* where the wind speed is below the rated speed and the turbine is ramping up.
(ii) Steady state (1500 *RPM)* where the turbine has achieved its rated speed and is generating power.

For the minimum reflection coefficient plot (which is an indication of lubricant film thickness) the trend resembles a Stribeck curve. At low rotational speeds, R increases briefly before decreasing and finally increasing steadily until reaching the rated speed of 1500 *RPM*. The minimum reflection coefficient then exhibits a range of values at 1500 *RPM*; this is due to an increase in bearing load as the turbine starts generating power. This load increase is observed in the maximum roller load data at 1500 *RPM*. The trend of R_{min} is also consistent for both channels across the rotational speed, with an offset between the two channels due to the sensor positioning within the loaded zone.

The load data, Q_{max}, shows an interesting feature; at low speed (0–1300 *RPM*) CH1 is higher than CH2, despite the fact that is nominally in the low loaded region of the bearing. At around 1300 *RPM*, both CH1 & CH2 exhibit a step increase, with CH2 exceeding CH1. This is potentially due to high measurement error at <1300 *RPM* as the load on the bearing is small, and the error proportion reduces as the load increases.

The load increase and conversely decrease in minimum reflection coefficient (film thickness) at steady state is due to an increase in wind speed. This would have a strong effect on the bearing life. Within the measurements observed in Fig. 15, the roller load varies from 1.5 to 7 kN. Taking a mean load of 4.25 kN as reference and assuming same life modification factors (a_1 & a_{ISO}), the bearing fatigue life, L_{10} calculated through ISO 281:2007 standard [26] was seen to decrease more than 5 fold as the roller load increases from 4.25 to 7 kN, highlighting the significant impact of increasing wind speed on fatigue life.

5.5. Roller lubrication and lubricant reflow time

As explained in §4.3, reflection coefficient measurements in the gap between roller passes contain information on the lubrication state of the raceway and subsequently the roller. Figs. 10 and 11 showed how the value of R (either 0.95 or 1) could indicate whether the raceway was fully flooded with oil or exposed to air. It is important to note that when $R = 1$ this does not necessarily means that there is absolutely no oil present on the raceway. A very thin layer of oil (less than about 150 μm or so) will not be detectable and would also lead to a measurement close to unity. Rather $R = 1$ indicates that the raceway is just not fully flooded.

In Figs. 10 and 11 a region of low reflection is observed immediately after the roller passage as the oil is swept away from the raceway. In Fig. 16, this 'reflow' time has been correlated with the rotational speed of the bearing. The reflow time reduces exponentially as the rotational speed increases. It is apparent that due to the lubricant reflow mechanism at low rotational speed, the reflow time varied significantly compared to that obtained at higher rotational speed. During instances

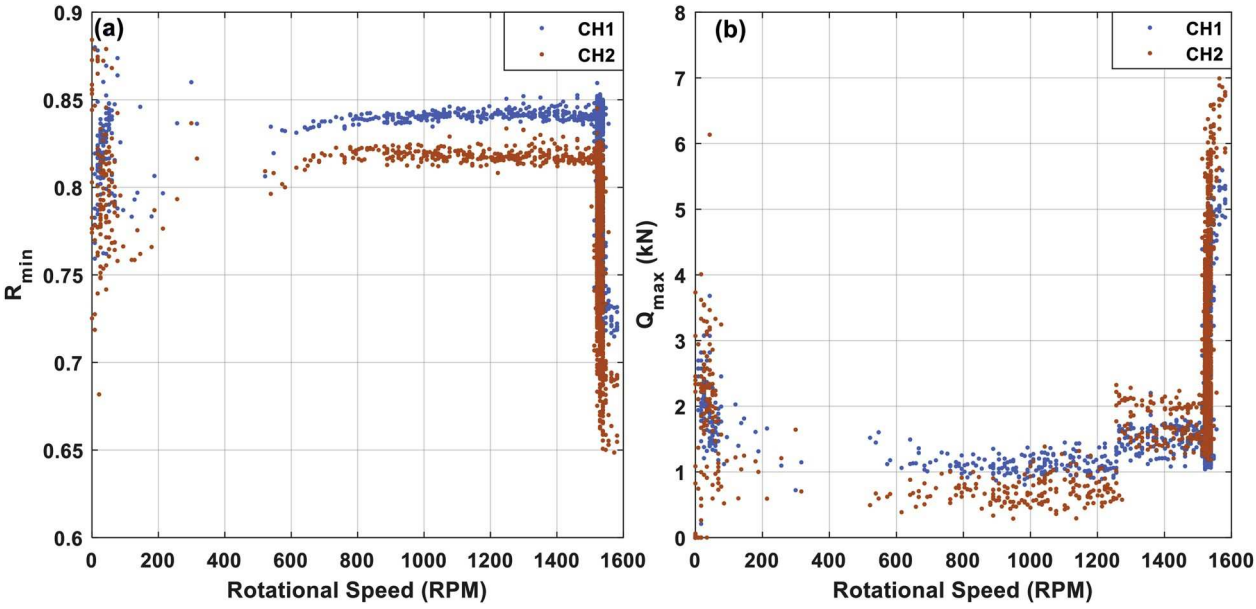

Fig. 15. Variation of (a) minimum reflection coefficient and (b) maximum roller load with bearing rotational speed.

of low bearing rotation, the lubricant has sufficient time to reoccupy the region previously swept clean by a roller before the subsequent roller passes through. At higher speeds, the reduction of lubricant reflow time is due to the increase in rotational speed as the roller pushes the lubricant into the starved raceway region ahead of its passage.

Fig. 17 shows one particular set of data that captures two distinct lubrication phenomenon within a single revolution. For the first 5 roller passes, the reflection coefficient between roller passes remains at 1 indicating reduced (i.e. not fully flooded) lubrication. For the subsequent 5 roller passes, the reflection coefficient exhibit the more normal "zig-zag" pattern where it transitions from insufficient to adequately lubricated. In this design, oil is fed into the top of the gearbox and relies on the rotating parts to distribute it around the bearings. It would appear that the process is non-stationary and prone to intermittent lubrication.

It is important that the roller and raceway interface are lubricated to reduce metal-metal contact. Increased solid contact would result in wear and higher local stresses in the near surface region, leading to bearing failure. When the rolling surfaces are intermittently lubricated, there exist instances where metal-metal contact occur which increases the risk of rolling surface damage and subsequently premature failure. At such instances, bearing life would be significantly reduced. Research conducted by two bearing companies [27,28] demonstrated that lambda ratio, lubricant inlet starvation and low viscosity ratio have an adverse effect on bearing life. A separate study [29] found that significant wear occurs when the lubricant film is interrupted, demonstrating the impact of intermittent lubrication.

6. Discussion

6.1. Qualitative comparison of load measurements

The method for the deduction of roller load from ultrasonic reflection measurements has been validated on a full-scale rig in the laboratory [13]. However, there is a scarcity of published work on in-situ measurement of WT bearing loads, so possibilities for the validation of the field data is limited. The following paragraphs will attempt to

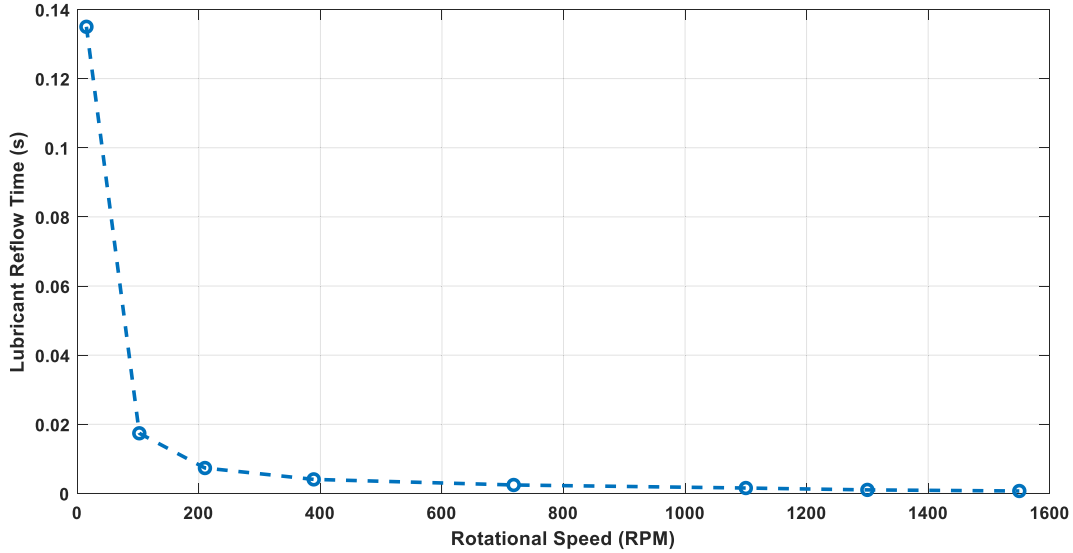

Fig. 16. Variation of lubricant reflow time with rotational speed.

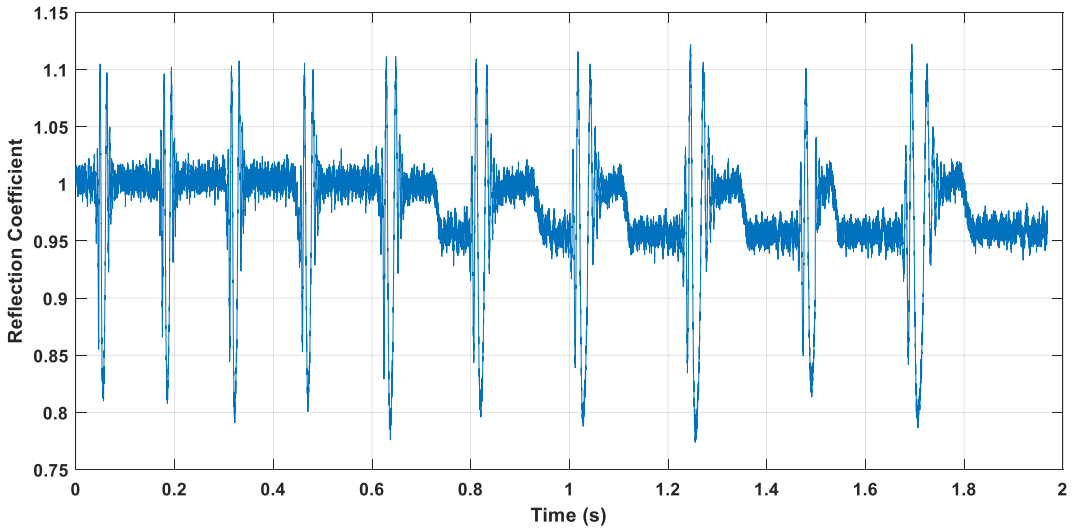

Fig. 17. An indication of roller lubrication; a single data set where the first 5 roller passes sweep out oil and are not replenished. For the next 5 roller passes, replenishment occurs.

qualitatively compare the load data measured in this work with modelling and measurement results from two investigations [30,31].

The two published studies [30,31] have sought to model and measure the loads on the high-speed shaft bearings during normal operation. In both cases, the studies were performed on NREL's 750 kW gearbox. The NREL gearbox has a higher rating (750 kW compared to 600 kW in this study) and slightly different shaft layout (the location of the TRB pair and the single cylindrical roller bearing (CRB) are on opposite sides of the pinion) to the one in the present study. As a result of these differences, only qualitative comparisons can be made with the load data measured in this work.

In Bruce et al. [30], a multibody dynamic wind turbine gearbox model was developed using Ricardo's VALDYN software to simulate the 750 kW NREL turbine drivetrain. The model requires information on the mass, inertia, damping, material properties as well as dimensions of gearbox components as inputs and resolves the torque, reaction forces of the gearbox components and the bearings internal stresses and strains. The model however is unable to simulate load sharing between the planetary gear bearing pairs, rotor and generator off-axis loads and also the gearbox component's internal deflections. The resultant forces of the HSS bearings computed by the model are summarised in Table 3.

In Guo and Keller [31], three models of increasing complexity (semi-analytical, SIMPACK multi-body, and Transmission 3D finite element models) were used to deduce bearing loads for the same 750 kW NREL drivetrain. The modelling results were subsequently compared with a dynamometer test, in which the HSS TRB pair was instrumented with strain gauges to measure bearing load. Apart from transitional operation, the experimental and modelling results agree well with each other. As the generator power was increased, a linear trend was also observed for the HSS bearing load. The radial load of the HSS bearings at maximum power is shown in Table 3. Individual TRBs radial load were not made available in the paper, however the authors noted that the downwind TRB bears a higher load due to it supporting most of the axial load.

Since the CRB only supports radial load and the two studies are simulating the same drivetrain, load measurement results for the cylindrical bearing should be similar across the two studies. However, measurements vary by 16 kN. Results from Ref. [31] bear higher confidence due to the modelling results agreeing with the experimentally measured load from the dynamometer test. The discrepancy is potentially resulted from the limitations of the model mentioned previously.

For the current study, a 20.6 kN bearing load measured at 356 kW off the downwind TRB seems sensible compared with the two other studies.

Table 3
Comparison of field measured HSS bearing load with theoretical and laboratory-based experimental studies.

Present study	**Bearing**	**Bearing Radial Load (kN) at 356 kW**
	TRB-Downwind	20.6
Bruce et al. [30]	**Bearing**	**Total Bearing Load (kN) at 750 kW**
	CRB	63.0
	TRB-Downwind	79.0
	TRB-Upwind	15.0
Guo & Keller [31]	**Bearing**	**Bearing Radial Load (kN) at 750 kW**
	CRB	47.0
	TRB-Pair (Down & Upwind)	31.0

Since only the downwind bearing of the TRB pair was instrumented, comparison across the HSS bearing was not possible for this current study.

6.2. *Limitations and assumptions*

The measurement approach developed in this study has a number of limitations and assumptions which are explored in this section.

The ultrasonic load measurement technique infers raceway deformation from change in time-of-flight and requires a contact model to convert raceway deformation into roller load and subsequently bearing load. For simple geometries, i.e. cylinder on flat surface, it is relatively straight forward to select the appropriate contact model. However, when there exists roller and raceway profiles in addition to their major radii, this becomes more complex. The contact will be elliptical at low loading and gradually transition into line contact at high loads. The primary challenge would be to determine the roller and raceway profiles, typically at the micrometre scale, and evaluate an equivalent reduced radius for the two profiles. This would require measurements using a surface profilometer or a coordinate measurement machine, as bearing manufacturers are reluctant to provide this sensitive information.

The acoustoelastic constant of bearing steel was found to have an uncertainty of $<5\%$ [13]. This arose during the first loading and unloading cycle due to plastic deformation of the bearing steel. However, during the subsequent cycles, the value stabilized at -2.24. As the

HSS bearing is under low loading (<10% of the bearing's dynamic load rating), it is not expected that the raceway would plastically deform and thus the acoustoelastic constant for the bearing would not vary and affect the roller load measurements.

Temperature variation will affect the speed of sound as ultrasonic waves propagate through the bearing raceway and subsequently the ToF measurements. This was accounted for through data processing means detailed in §4.1. A distinct reference pulse is obtained from each dataset, i.e. a dataset recorded in summer at a particular temperature would have a reference pulse at that same temperature. Consequently, this 'live' acquisition of reference accounted for temperature variations during bearing operation and throughout the change in seasons.

With the current sensor data acquisition method, a reference pulse is taken when a roller is not directly located beneath the sensor. It is then assumed that the raceway is unloaded. This method of acquiring a reference is only valid when there is no residual stresses present within the raceway. The presence of residual stresses within the bearing raceway can be roughly evaluated through comparing the unstressed speed of sound measurements of two sensors at two locations around the circumference of the bearing. A difference greater than 5% between the two measurements indicate the presence of residual stress within either one of the measured locations.

Two raceway lubrication conditions exist when obtaining a reference pulse. If a reference pulse is chosen when the raceway is un-lubricated, i.e. steel-air, the reflection coefficient measurements will be true whereas when a lubricated reference is taken, the reflection coefficient values will require multiplication by 0.95 to be valid as the reflection coefficient value for a steel-oil interface is 0.95. Often enough, patterns within a particular dataset will exhibit clues to which whether the shifting of the reflection coefficient is necessary.

For optimum sensor response and wiring requirements, the minimum width of the piezo-ceramic sensor is limited to around 1 mm. Taking beam spread into account, the sensing region of the transducer would be in the region of 3 mm. This is still relatively large compared to the raceway-roller contact size of less than 0.5 mm and since measurements obtained are averaged across all the pulses captured within the sensing region, detailed information of the contact region is not possible.

The amount of free surface lubricant film thickness required to register a reflection coefficient of 0.95 is currently less understood. It is theorized that as the free surface lubricant film thickness decreases, the reflection coefficient will gradually increase from 0.95 until unity. In principle a free surface film thinner than the wavelength of the ultrasonic wave will not be detectable by the ultrasonic sensor and thus registers a reflection coefficient of unity.

Presently, the averaging effect of the sensor on the load measurements is a subject of further research. It is believed that the load reading is an averaged value measured across the transducer sensing region, however laboratory validation testing of a cylindrical roller loaded between two plates seem to indicate that this does not affect the accuracy of the ultrasonic load measurement technique. As only two sensors were instrumented on the static outer raceway, the bearing circumferential load resolution is only limited to these two points. For static raceway instrumentation, the higher the amount of sensors installed, the better the circumferential load resolution. An alternative method of reducing instrumentation requirement would be instrumenting the rotating part, i.e. the inner raceway. One sensor would then be sufficient to map out the circumferential load. However, slip rings would be required which adds complexity to the instrumentation process. The accuracy of the load measurement technique is affected by the lateral and vertical sampling resolutions; lateral referring to the time resolution and vertical being the signal amplitude or voltage resolution. The higher the two resolutions, the better the accuracy. Signal-to-noise ratio also plays an important role, at low load the change in ToF is very small and thus measurements are of susceptible to larger errors. This improves as the load gradually increases. Currently, the smallest measurable change in ToF with reasonable confidence in signal-to-noise ratio is 1.70 ns (1 kN), with a smallest detectable deflection of 0.02 μm, recorded using a 10 ns digitizer.

There are a number of complexities associated with the installation of the measurement system. The sensors need to be positioned normal to the loading region to allow sound waves to propagate perpendicular towards the contact interface. For a tapered roller contact as used in this study, this requires machining the bearing to accommodate the sensors; and alternative would have been the use of an angled boss. The intricacies involved in installing sensors onto the raceway is further complicated by the difficulty of accessing key strategic regions within the bearing. The presence of a bearing housing and limited space within the nacelle restrict available regions for sensor positioning and cable routing. As a result, retrofitting of ultrasonic sensors is unlikely to be possible without sufficient access to a bearing. In this study, due to complexity and access restrictions in instrumenting a higher loaded bearing, such as a planetary bearing, an easier, more accessible, low loaded HSS bearing was retrofitted instead.

Although attempt was taken to reduce the amount of data generated through capturing 1 s of data every 20 min, large amounts of data were still accumulated. This is partially due to the high PRR required, generating a 50 MB size data each capture. However, measurements were often captured when the turbine was idle resulting in superfluous data. A better acquisition configuration would be to capture data during turbine transient events only, as these result in the most damage to the bearings. This could be achieved by reading turbine operating parameters such as generator torque or wind speed and triggering the acquisition PC to capture when they are fluctuating excessively.

Notwithstanding the above, the approached has proved capable of measuring, for the first time, the load directly imparted by each roller on the raceway and indicated how this is very likely to be dependent on the geometry of the rolling element. The flow of lubricant around the bearing has also been measured in a qualitative way and shown some interesting phenomenon. Above all, the use of relatively low cost piezo-ceramic sensors for ultrasonic measurement, partially alleviates any economic considerations and does not inhibit large amount of sensors to be instrumented onto the raceway.

7. Conclusions

The high-speed shaft bearing in an operational wind turbine gearbox was instrumented by bonding piezo-electric ultrasonic sensors onto the outer raceway. The sensors were used to generate ultrasonic pulses that were reflected from the raceway-roller contact and recorded by the same sensor.

The reflected ultrasonic signal was analysed in two ways. Firstly, the time of flight of the pulse travelling to the raceway roller contact was recorded as rollers swept past the measurement location. This ToF reduced as the raceway was compressed by roller passage. This was used to determine the load imparted by each roller onto the raceway. Secondly, the amplitude of the reflected signal compared to the incident wave (the Reflection Coefficient) was recorded. This was used to qualitatively measure the amount of lubrication around the bearing circumference.

Key findings of this study include:

(i) The lubrication film generated by the same roller within a complement is consistent with each revolution, however there are very slight variations within the complement.
(ii) The load carried by the same roller within a complement varied less with each revolution compared to that of all the rollers across the complement. This load variation between different rollers is believed to be caused by slight variations in roller profile geometry.
(iii) Trends in measurements of reflection coefficient and roller load across two measurement channels are consistent. High load,

leading to thin oil films and possible surface contact, was commensurate with low reflection coefficient and vice versa.

(iv) Two regimes of bearing operation were identified when the reflection coefficient and roller load were plotted against bearing speed. As the turbine ramps up to rated speed, the minimum reflection coefficient increases gradually as more lubricant is entrained into the contact whilst no apparent trend was observed for the max roller load during this phase. The minimum reflection coefficient and maximum roller load then exhibit a range of values at rated speed as the turbine starts generating power.

(v) Two lubrication reflow behaviours were observed at low and high bearing rotational speeds. At low rotational speeds, the lubricant is allowed sufficient time to flow back into the region previously swept clean by the roller. At high rotational speeds, the lubricant is forced into the region by the incoming roller. There were occasions in the measurement set where certain rollers did not have a fully flooded inlet, whilst near neighbours did. This demonstrates the stochastic nature of the bearing lubrication.

Declaration of competing interest

The authors declare that they have no known competing financial interests or personal relationships that could have appeared to influence the work reported in this paper.

CRediT authorship contribution statement

G. Nicholas: Formal analysis, Investigation, Writing - original draft, Writing - review & editing, Visualization. **T. Howard:** Conceptualization, Methodology, Data curation. **H. Long:** Writing - review & editing. **J. Wheals:** Supervision, Project administration. **R.S. Dwyer-Joyce:** Resources, Writing - original draft, Writing - review & editing, Supervision, Project administration, Funding acquisition.

Acknowledgements

The authors would like to acknowledge the helpful advice and comments from Dr Ed Hart of Strathclyde University, Dr Dalil Benchebra of Ricardo Ltd, and Dr Luc Houpert of the Timken Company. In addition, the authors would like to acknowledge the financial support of the Engineering and Physical Sciences Research Council for funding this research through Professor Dwyer-Joyce's fellowship on *Tribo-Acoustic Sensors* EP/N016483/1 and the *Centre for Doctoral Training in Integrated Tribology* EP/L01629X/1.

Appendix A. Supplementary data

Supplementary data to this article can be found online at https://doi.org/10.1016/j.triboint.2020.106322.

References

[1] European Wind Energy Association [EWEA]. Pure Power, wind energy targets for 2020 and 2030. Available from, http://tiny.cc/j0k18y; 2011.
[2] Faulstich S, Hahn B, Jung H, Rafik K. Suitable failure statistics as a key for improving availability. Proc EWEC 2009;7:4592–600.
[3] Hahn B, Durstewitz M, Rohrig K. Reliability of wind turbines, experiences of 15 Years with 1,500 WTs. Wind Energy; 2007.
[4] Kotzalas M, Doll G. Tribological advancements for reliable wind turbine performance. Phil Trans Math Phys Eng Sci 2010;368(1929):4829–50.
[5] Kim K, Parthasarathy G, Uluyol O, Foslien W, Sheng S, Fleming P. Use of SCADA data for failure detection in wind turbines. In: ASME 2011 5th international conference on energy sustainability; 2011.
[6] Musial W, Butterfield S, McNiff B. Improving wind turbine gearbox reliability. European Wind Energy Conference; 2007.
[7] Hameed Z, Hong YS, Cho YM, Ahn SH, Song CK. Condition monitoring and fault detection of wind turbines and related algorithms: a review. Renew Sustain Energy Rev 2009;13(1):1–39.
[8] Chakrapani S, Dayal V, Krafka R, Eldal A. Ultrasonic testing of adhesive bonds of thick composites with applications to wind turbine blades. AIP Conf Proc 2012; 1430:1284–90.
[9] Li S, Shi K, Yang K, Xu J. Research on the defect types judgement in wind turbine blades using ultrasonic NDT. In: Global conference on polymer and composite materials; 2015.
[10] Tchakoua P, Wamkeue R, Tameghe TA, Ekemb G. A review of concepts and methods for wind turbines condition monitoring. World Congress on Computer and Information Technology; 2013.
[11] Dwyer-Joyce R, Drinkwater B, Donohoe C. The measurement of lubricant-film thickness using ultrasound. Pro Roy Soc A 2003;459(2032):957–76.
[12] Dwyer-Joyce R, Reddyhoff T, Drinkwater B. Operating limits for acoustic measurement of rolling bearing oil film thickness. Tribol Trans 2004;47(3):366–75.
[13] Chen W, Mills R, Dwyer-Joyce R. Direct load monitoring of rolling bearing contacts using ultrasonic time of flight. Pro Roy Soc A 2015;471(2180):1–21.
[14] Reddyhoff T, Kasolang S, Dwyer-Joyce R. The phase shift of an ultrasonic pulse at an oil layer and determination of film thickness. Proc Inst Mech Eng 2005;219(6): 387–400.
[15] Zhang K, Meng Q, Zhao W. Measurement of oil film thickness in cylindrical roller bearing by ultrasound. In: Proceedings of the ASME 2014 12th biennial conference on engineering systems design and analysis; 2014.
[16] Geng T, Meng Q, Chen Z, Wang P. Ultrasonic monitoring of lubricating conditions of hydrodynamic bearings. J Phys Conf 2011;305(1):012065.
[17] Li M, Liu H, Xu C, Jing M, Dong G. Ultrasonic measurement of cylindrical roller-bearing lubricant film distribution with two juxtaposed transducers. Tribol Trans 2017;60(1):79–86.
[18] Pialucha T, Guyott C, Cawley P. Amplitude spectrum method for the measurement of phase velocity. Ultrasonics 1989;27(5):270–9.
[19] Dwyer-Joyce R, Reddyhoff T, Zhu J. Ultrasonic measurement for film thickness and solid contact in elastohydrodynamic lubrication. J Tribol 2011;133(3):031501.
[20] Zhang J, Drinkwater B, Dwyer-Joyce R. Acoustic measurement of lubricant-film thickness distribution in ball bearings. J Acoust Soc Am 2006;119(2):863–71.
[21] Dwyer-Joyce R, Reddyhoff T. Ultrasonic measurement of EHL oil films in a mixed regime contact. STLE/ASME 2006 International Joint Tribology Conference; 2006.
[22] Houpert L. An engineering approach to hertzian contact elasticity – Part I. J Tribol 2001;123(3):582–8.
[23] Houpert L. Hydrodynamic load calculation in rolling element bearings. Tribol Trans 2016;59(3):538–59.
[24] Howard T. Development of a novel bearing concept for improved wind turbine gearbox reliability. PhD Thesis. University of Sheffield; 2016.
[25] Harris TA. Rolling bearing analysis. fourth ed. John Wiley & Sons; 2001.
[26] ISO 281:2007. Rolling bearings – dynamic load ratings and rating life. International Organisation for Standardisation; 2007.
[27] Chiu Y. The dependence of rolling bearing surface fatigue on lambda ratio and other variables. SAE Trans 1994;103(2):236–42.
[28] Morales-Espejel G, Gabelli A, Ioannides E. Micro-geometry lubrication and life ratings of rolling bearings. Proc IME C J Mech Eng Sci 2010;224(12):2610–26.
[29] Tallian T, Chiu Y, Huttenlocher D, Kamenshine J, Sibley L, Sindlinger N. Lubricant films in rolling contact of rough surfaces. ASLE Trans 1964;7(2):109–26.
[30] Bruce T, Long H, Dwyer-Joyce R. Dynamic modelling of wind turbine gearbox bearing loading during transient events. IET Renew Power Energy 2015;9(7): 821–30.
[31] Guo Y, Keller J. Investigation of high-speed shaft bearing loads in wind turbine gearbox through dynamometer testing. Wind Energy 2018;21(2):139–50.